Structure and function of an effector domain in antiviral factors and tumor suppressors SAMD9 and SAMD9L

Shuxia Peng[a,1], Xiangzhi Meng[b,1], Fushun Zhang[b,1], Prabhat Kumar Pathak[a], Juhi Chaturvedi[a], Jaime Coronado[b], Marisol Morales[b], Yuanhui Mao[c], Shu-Bing Qian[c], Junpeng Deng[a,2], and Yan Xiang[b,2]

[a]Department of Biochemistry and Molecular Biology, Oklahoma State University, Stillwater, OK 74078; [b]Department of Microbiology, Immunology and Molecular Genetics, University of Texas Health Science Center at San Antonio, San Antonio, TX 78229; and [c]Division of Nutritional Sciences, Cornell University, Ithaca, NY 14853

Edited by Ian Wilson, Integrative Structural and Computational Biology, Scripps Research Institute, La Jolla, CA; received September 8, 2021; accepted December 8, 2021

SAMD9 and SAMD9L (SAMD9/9L) are antiviral factors and tumor suppressors, playing a critical role in innate immune defense against poxviruses and the development of myeloid tumors. SAMD9/9L mutations with a gain-of-function (GoF) in inhibiting cell growth cause multisystem developmental disorders including many pediatric myelodysplastic syndromes. Predicted to be multidomain proteins with an architecture like that of the NOD-like receptors, SAMD9/9L molecular functions and domain structures are largely unknown. Here, we identified a SAMD9/9L effector domain that functions by binding to double-stranded nucleic acids (dsNA) and determined the crystal structure of the domain in complex with DNA. Aided with precise mutations that differentially perturb dsNA binding, we demonstrated that the antiviral and antiproliferative functions of the wild-type and GoF SAMD9/9L variants rely on dsNA binding by the effector domain. Furthermore, we showed that GoF variants inhibit global protein synthesis, reduce translation elongation, and induce proteotoxic stress response, which all require dsNA binding by the effector domain. The identification of the structure and function of a SAMD9/9L effector domain provides a therapeutic target for SAMD9/9L-associated human diseases.

myeloid malignancies | poxvirus | innate immunity | myelodysplasia syndrome | NOD

Sterile Alpha Motif Domain–containing 9 (SAMD9) and its paralog SAMD9L (SAMD9/9L) are tumor suppressor genes tandemly located on human chromosome 7. A multisystem developmental disorder named MIRAGE syndrome (myelodysplasia, infection, restriction of growth, adrenal hypoplasia, genital phenotypes, and enteropathy) is caused by mutations in SAMD9 (1), while ataxia-pancytopenia (2) and a similar disease with immunodeficiency and variable neurological presentation (3) are caused by mutations in SAMD9L. These disorders are autosomal dominant and associated with missense mutations of SAMD9/9L that exhibit a gain of function (GoF) in inhibiting cell proliferation. Similar GoF missense mutations represent the most frequent genetic cause for the inherited bone marrow failure syndromes (4). Moreover, frameshift mutations that truncate nearly the C-terminal half of SAMD9L were recently found to be associated with systemic autoinflammatory diseases and display a GoF in restricting cell growth (5–7). Individuals harboring GoF SAMD9/9L mutations are predisposed to myelodysplastic syndromes and monosomy 7 (8), a cytogenetic abnormality frequently associated with myeloid malignancies (9). The loss of the chromosome 7 carrying the GoF SAMD9/9L mutations from bone marrow cells was suggested to be an "adaption by aneuploidy" to restore hematopoiesis while simultaneously predisposing to myeloid malignancies (10). Indeed, haploinsufficiency of SAMD9L contributes to myeloid transformation in a mouse model (11).

SAMD9/9L have also been implicated in antiviral defense against several viruses, most prominently poxviruses (12–14). SAMD9/9L are ubiquitously expressed in many tissues (15), and their expression can be further induced by interferons. Nearly all mammalian poxviruses encode at least one specific inhibitor against SAMD9/9L, with the prototypical poxvirus vaccinia encoding two inhibitors that target different regions of SAMD9/9L (16, 17). The deletion of both SAMD9/9L inhibitors, K1 and C7, from vaccinia virus resulted in abortive replication in most mammalian cells due to a shut-off of global protein synthesis (18–20).

SAMD9/9L are large cytoplasmic proteins with more than 1,500 amino acids (aa). They are predicted to contain multiple domains with an architecture reminiscent of Apaf-1 and NOD-like receptors (21), which are self-regulated signaling molecules containing separate sensor and effector domains. However, the molecular and structural basis for the diverse functions of SAMD9/9L are unknown. Here, we identified a 230-aa effector domain in SAMD9 that binds preferentially to double-stranded (ds) nucleic acids (dsNA) and determined its crystal structure in complex with DNA. Utilizing precise mutations that disrupt

Significance

SAMD9 and SAMD9L (SAMD9/9L) are important innate immune defenders against viruses and the development of myeloid tumors. They form a crucial host barrier that poxviruses must overcome for successful infection. A myriad of human diseases including many pediatric myelodysplastic syndromes are caused by mutations in SAMD9/9L. However, the molecular functions of SAMD9/9L and how their functions are executed are unknown, hindering progress in developing effective therapies for SAMD9/9L-associated human diseases. Here, we identified the structure and function of a SAMD9/9L effector domain that is essential for their physiological functions as well as the pathogenic effects exerted by patient-derived mutations. Our study revealed a potential therapeutic target for SAMD9/9L-associated human diseases.

Author contributions: J.D. and Y.X. designed research; S.P., X.M., F.Z., P.K.P., J. Chaturvedi, J. Coronado, and M.M. performed research; Y.M., S.-B.Q., J.D., and Y.X. analyzed data; and J.D. and Y.X. wrote the paper.

The authors declare no competing interest.

This article is a PNAS Direct Submission.

[1]S.P., X.M., and F.Z. contributed equally.

[2]To whom correspondence may be addressed. Email: xiangy@uthscsa.edu or Junpeng.deng@okstate.edu.

This article contains supporting information online at http://www.pnas.org/lookup/suppl/doi:10.1073/pnas.2116550119/-/DCSupplemental.

Published January 19, 2022.

dsNA binding to different degrees, we demonstrated that dsNA binding is essential for the seemingly diverse functions of SAMD9/9L in tumor suppression, antiviral responses, and translation control.

Results

Identification of a dsNA Binding Domain in SAMD9. SAMD9 aa 195 to 352 bears some sequence similarity to the NA-binding Alba domain (21). Based on our secondary structure analysis, a larger SAMD9 region of aa 134 to 385 ($SAMD9^{134\text{-}385}$) was expressed and purified to assess its binding to NA with the electrophoresis mobility shift assay (EMSA). $SAMD9^{134\text{-}385}$ formed stable complexes with synthetic dsRNA and dsDNA of various lengths from 18- to 30-nucleotide (nt) but not with an 11-nt dsDNA (*SI Appendix*, Fig. S1*A*). Optimal complex formation appeared to be achieved when the protein and DNA were mixed at 2:1 molar ratio (*SI Appendix*, Fig. S1*B*). The binding of $SAMD9^{134\text{-}385}$ with a fluorescence-labeled dsDNA can be effectively competed off with unlabeled dsDNA, dsRNA, and poly I:C but only slightly with single-stranded (ss) RNA and ssDNA (*SI Appendix*, Fig. S1*C*), indicating that $SAMD9^{134\text{-}385}$ preferentially binds dsNA.

The Crystal Structure of $SAMD9^{156\text{-}385}$ in Complex with DNA. Through limited proteolysis of $SAMD9^{134\text{-}385}$, a smaller domain that retained the dsNA binding activity was identified (*SI Appendix*, Fig. S2 *A* and *B*). The compact domain of $SAMD9^{156\text{-}385}$ can be crystallized with a 22-nt dsDNA, and the complex crystal structure was determined at 2.8-Å resolution. Although purified as a monomer, the protein DNA complex is estimated to be a dimer by gel filtration (*SI Appendix*, Fig. S2*C*). Consistently, one asymmetric unit of the crystal lattice contains two protein molecules situated on the opposite sides of a canonical B-form dsDNA helix (Fig. 1 *A* and *B*). The two protein protomers are related by a noncrystallographic twofold symmetry that is perpendicular to the DNA axis. One protomer is shifted along the DNA axis by 8 nt with respect to the other (Fig. 1*B*). Together, the dimer covers 22 nt of DNA in length with nearly no protein–protein contacts.

The structures of the two protomers closely resemble each other with an RMSD of 0.42 Å over 207 aligned residues. The structure is compact and mainly comprises six α-helices and 14 β-strands with an overall dimension of ~53 × 33 × 30 Å. Most of the β-strands are short with 2 to 3 aa except for β-4, β-5, β-9, and β-10, which form a central β-sheet together with β-8, packed by five short strands (β-1, β-2, β-3, β-6, and β-7) on one side and by three α-helices (α-1, α-2 and α-3) on the opposite side. The 10 β-strands together form an asymmetrical β-barrel. Two short β-hairpins (β-11 to β-12 and β-13 to β-14) and three additional helices (α-4, α-5, and α-6) are present at the C terminus (Fig. 1*C*). The loops between β-3 and β-4, β-9 and β-10, and β-11 and β-12 are disordered. The central β-sheet and helices α-1 and α-2 resemble an Alba domain fold (22), but the overall structure does not have any close match when searched using the Secondary Structure Matching (SSM) server (23).

$SAMD9^{156\text{-}385}$ mainly contacts the phosphate backbone of the DNA without interacting with any DNA bases, suggesting a sequence-independent binding mode. In both protomers, charge–charge interactions with the DNA cluster at three basic residues, K198 located on the loop β-4 to α-1 and K214 and R221 located on helix α-1. In protomer A, K198 forms a salt bridge with the nonbridging oxygen of the backbone phosphate at the nucleotides T7 to A8. K214 contacts the DNA backbone at the nucleotides A8 to A9. R221 contacts the nucleotides T11 to C12 in the other DNA strand (Fig. 1*D*). In protomer B, both K198 and K214 contact the DNA backbone at the T7 to A8 in the other strand, while R221 contacts the DNA backbone at the A12 to T13. Additional contacts between the protein and the backbone of the DNA are observed from the side chains of K242 on loop β-6 to β-7 and K350 on strand β-14. These five basic residues are also highly conserved among SAMD9/9L family members (*SI Appendix*, Fig. S3*A*). Human SAMD9 and SAMD9L share ~60% aa identity, and a model structure of the corresponding domain of SAMD9L was established based on this homology (*SI Appendix*, Fig. S3*B*). We hereafter refer $SAMD9^{156\text{-}385}$ and the corresponding region in the SAMD9/9L family as the dsNA-binding domain (DBD).

Mechanism of DNA Binding by SAMD9 DBD. We selected the five conserved basic residues observed to contact DNA (K198, K214, R221, K242, and K350) and an additional conserved basic residue (K257) far away from the DNA interface for mutagenesis studies. The residues were individually substituted with glutamate to reverse the charge of the side chains. DNA binding by $SAMD9^{134\text{-}385}$ in EMSA was not affected by K257E substitution, while it was completely disrupted by the K198E, K214E, and R221E substitutions and partially disrupted by the K242E and K350E substitutions, indicating that residues K198, K214, and R221 each play an essential role, while K242 and K350 are only partially required for DNA binding (Fig. 1*E*). The binding affinity of $SAMD9^{134\text{-}385}$ with the 22-nt dsDNA was determined to be ~16 μM by the fluorescence polarization assay (Fig. 1*F*). The binding affinity was similarly affected by the substitutions as in EMSA, except that the K214E mutant showed a low but better than expected binding affinity (~222 μM).

DBD dsNA Binding Activity Is Essential for the Antiviral Effect of the Wild-type (WT) and GoF SAMD9/9L Variants. Having defined a set of DBD mutations that reduce dsNA binding to different levels, we next utilized these mutations to assess the importance of dsNA binding in SAMD9/9L functions. We first studied the effects of the DBD mutations on the antiviral activities. A vaccinia virus mutant deleted of the viral SAMD9/9L inhibitors ($vK1^-C7^-/GFP^+$) would replicate and express the green fluorescent protein (GFP) reporter only in cells that have no or low SAMD9/9L expression, including the human breast cancer BT20 and HEK 293T cells (12, 17). In BT20 cells that were transduced with a doxycycline-regulated SAMD9 transgene, productive viral replication rate (GFP^+%) was reduced by ~50% after the transgene was specifically induced (*SI Appendix*, Fig. S4*A*). By contrast, productive replication was reduced by ~30% by the K242E mutant and not affected by the K214E and R221E mutants, correlating with the effects of the mutations on dsNA binding. Although the K257E mutant had no defect in dsNA binding, it was also defective at inhibiting viral replication, indicating that the conservative K257 residue plays a separate but essential role for SAMD9 function. To further evaluate the mutants' effect on viral replication, we also performed the traditional viral growth assay. The yield of $vK1^-C7^-$ at 24 h postinfection was reduced by ~10-fold in BT20 cells that were induced to express the WT or K242E mutant, while it was not reduced in cells expressing similar levels of the K214, R221E, or K257E mutants (*SI Appendix*, Fig. S4*A*). A more pronounced antiviral effect was observed in clonally selected SAMD9-expressing cells, where the 24-h yield of $vK1^-C7^-$ was reduced by more than 100-fold by the WT SAMD9 while not reduced by the K214E or R221E mutants (*SI Appendix*, Fig. S4*B*), confirming that the K214E and R221E mutations abolish the antiviral activity.

To assess antiviral activities of a wide variety of SAMD9/9L mutants at single-cell level (Fig. 2*A*), mCherry-SAMD9/9L fusion was transfected into 293T cells for 36 h followed by infection with $vK1^-C7^-$ for 15 h. $vK1^-C7^-$ infection rate (GFP^+%) in cells expressing different levels of SAMD9/9L ($mCherry^+$)

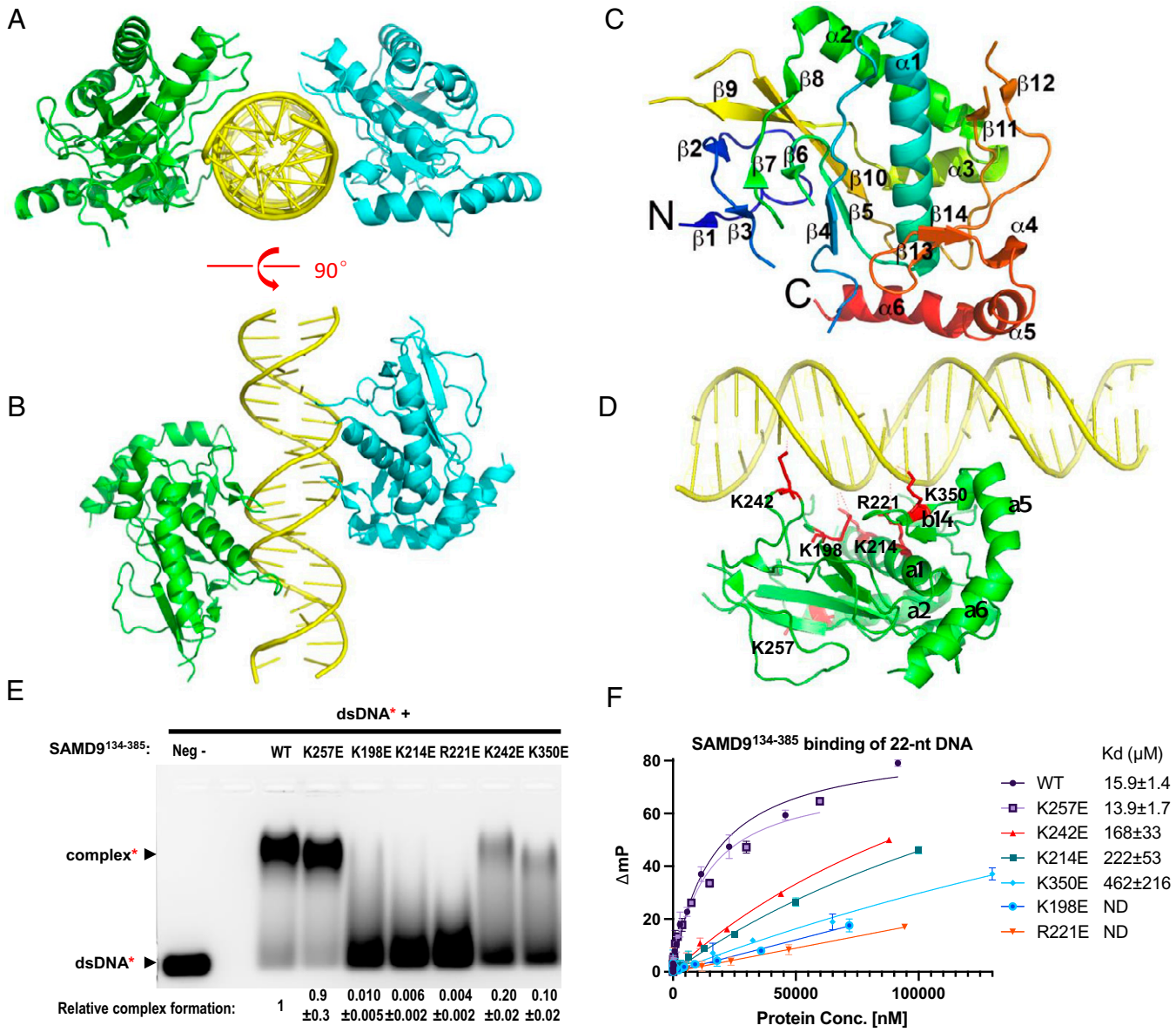

Fig. 1. The structure and molecular basis of DNA binding by SAMD9$^{156\text{-}385}$. (*A* and *B*) Perpendicular views of the crystal structure of SAMD9$^{156\text{-}385}$ dimer (green and cyan) in complex with a 22-nt dsDNA (yellow). (*C*) Secondary structures of SAMD9$^{156\text{-}385}$ are labeled and shown in rainbow color from blue to red starting from the N terminus. (*D*) SAMD9$^{156\text{-}385}$ primarily contacts the DNA backbone. Contacting residues (K198, K214, R221, K242, and K350) and a conserved noncontacting residue (K257) are shown as sticks and colored in red. The salt bridges are indicated as red dashed lines. (*E*) Purified SAMD9$^{134\text{-}385}$ proteins (WT or with specific mutations) were incubated with 5′ 6-FAM–labeled 22-nt dsDNA (indicated with red *) at 2:1 molar ratio and ran on an agarose gel. Florescence image of the gel is shown with locations where labeled DNA migrated are indicated. Relative intensities of the complex bands normalized to the WT level are shown with SD from three replicates. (*F*) 5′ 6-FAM–labeled 22-nt dsDNA was mixed with increasing concentrations of the proteins, and the change in fluorescence millipolarization (ΔmP) in response to protein concentrations is shown ($n = 3$). Binding affinities are derived from nonlinear fit of the data. Those for K198E and R221E could not be reliably determined (ND).

was quantified by flow cytometry (Fig. 2 *B* and *C*). Nontransfected cells (mCherry$^-$) from the same culture well served as the internal control. When substantial infection occurred in transfected cells, viral replication level as indicated by GFP intensity was also quantified (Fig. 2*D*). The infection rate and replication level were not reduced by the DBD-defective K198E, K214E, and R221E mutants, while they were reduced to different levels by the DBD partially defective K242E and K350E mutants (Fig. 2 *E* and *F*). Notably, the DBD-defective mutants failed to inhibit viral replication irrespective of their expression levels, but the cellular levels of the K242E and K350E mutants had a dose-dependent effect on their antiviral activities (Fig. 2*C*). More specifically, viral replication became nonpermissible only in cells that expressed a high level of the K350E mutant or an intermediate to high level of the K242E mutant (Fig. 2*C*, *Upper Right* quadrant), indicating that the partial defect of the two mutants can be overcome with overexpression. Overall, the effects of the DBD mutations on antiviral activities are similar in magnitude to their effects on dsDNA binding. The K257E mutant did not reduce the infection rate but decreased the viral replication level (Fig. 2 *D* and *F*), indicating that its antiviral activity is only partially defective, but the partial defect cannot be overcome with overexpression as in the case of K242E and K350E.

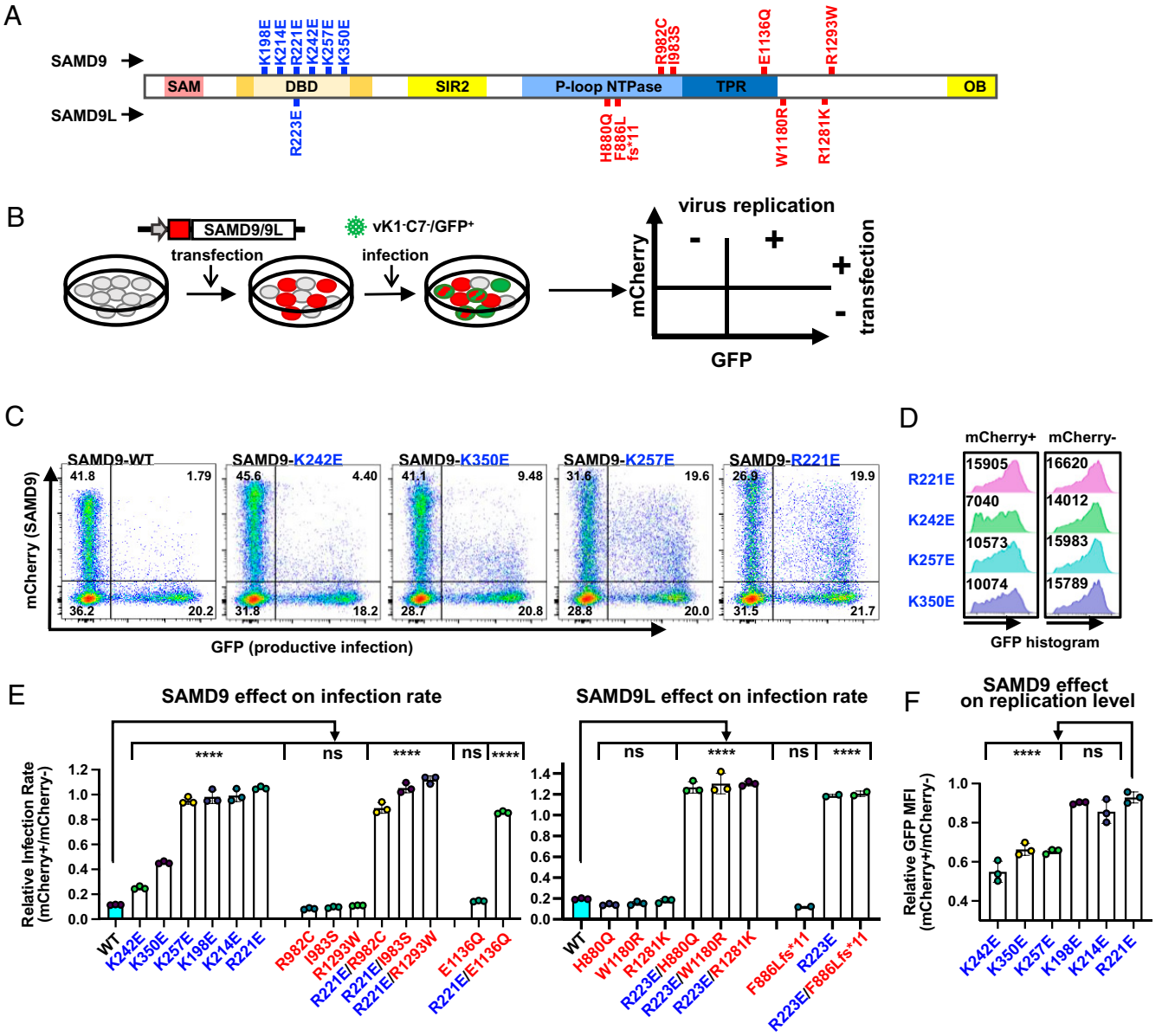

Fig. 2. dsNA binding by DBD is essential for antiviral activities of the WT and GoF SAMD9/9L variants. (*A*) The predicted SAMD9/9L domain architecture and the locations of GoF (labeled in red) and DBD (labeled in blue) mutations analyzed throughout the study. SAM, sterile alpha motif; DBD, dsNA-binding domain; SIR2, silent information regulator 2; P-loop NTPase, P-loop-containing nucleoside triphosphate hydrolase; TPR, tetratricopeptide repeats; and OB, oligonucleotide/oligosaccharide-binding. (*B*) HEK 293T cells were transfected with mCherry-SAMD9/9L fusions for 36 h and infected with vK1$^-$C7$^-$/GFP$^+$ for 15 h. Infection rates (GFP$^+$%) and replication levels (GFP MFI) among SAMD9/9L-expressing and nontransfected control cells from the same culture well were simultaneously determined with flow cytometry. (*C*) Representative flowcytometry plots with percentage of cells in each quadrant shown. (*D*) Representative GFP histograms of mCherry-SAMD9$^+$GFP$^+$ and mCherry$^-$GFP$^+$ cell populations with the GFP MFI shown. Relative infection rates (*E*) and replication levels (*F*) between SAMD9/9L-expressing and nontransfected cells are derived from the flow cytometry data shown in both Fig. 2 and *SI Appendix*, Fig. S5. Each biological replicate and SD are shown. Statistics: one-way ANOVA compared to the WT or R221E (ns, not significant; ****$P < 0.0001$).

To assess the relationship between the antiproliferative and antiviral activities, we next tested various patient-derived GoF SAMD9/9L variants (Fig. 2*A*), including R982C, I983S, E1136Q, and R1293W of SAMD9, and H880Q, W1180R, R1281K, and F886Lfs*11 of SAMD9L. They are representative of the pathogenic mutations identified in human patients, which predominately occur at the C-terminal half, particularly the putative NTPase domain (Fig. 2*A*). All the GoF variants, including the frameshifted SAMD9L^{F886Lfs*11}, displayed a similar inhibitory effect on vaccinia virus replication as the WT SAMD9/9L (Fig. 2 *E* and *F* and *SI Appendix*, Fig. S5). Also similarly, the antiviral effect of the GoF variants can be abolished by introducing the DBD-defective, R221E or the equivalent R223E mutation to SAMD9 or SAMD9L, respectively (Fig. 2*E* and *SI Appendix*, Fig. S3*B*). Altogether, our data showed that the DBD dsNA binding activity is critical for the antiviral effect of the WT and GoF SAMD9/9L variants.

DBD dsNA Binding Activity Is Essential for the Antiproliferative Activities of the WT and GoF SAMD9/9L Variants. To determine the impact of the DBD mutations on antiproliferative activities of SAMD9/9L, we transfected the mCherry-SAMD9/9L fusions into 293T cells and examined their effects on cell proliferation and cell cycle by quantifying the total as well as newly

synthesized DNA in the cells (Fig. 3 *A* and *B*). SAMD9L expression significantly reduced the number of proliferating, S-phase cells relative to that of the nontransfected cells from the same culture well (Fig. 3*B*), and the level of cellular DNA synthesis was reduced in a SAMD9L dose-dependent manner (Fig. 3*A*, *Upper Right* quadrant). SAMD9 had a similar effect, but a higher threshold of SAMD9 expression appeared to be required for reducing cellular DNA synthesis (*SI Appendix*, Fig. S6*A*). The GoF mutations enhanced the antiproliferative activity by varying degrees, with R982C of SAMD9 and the H880Q

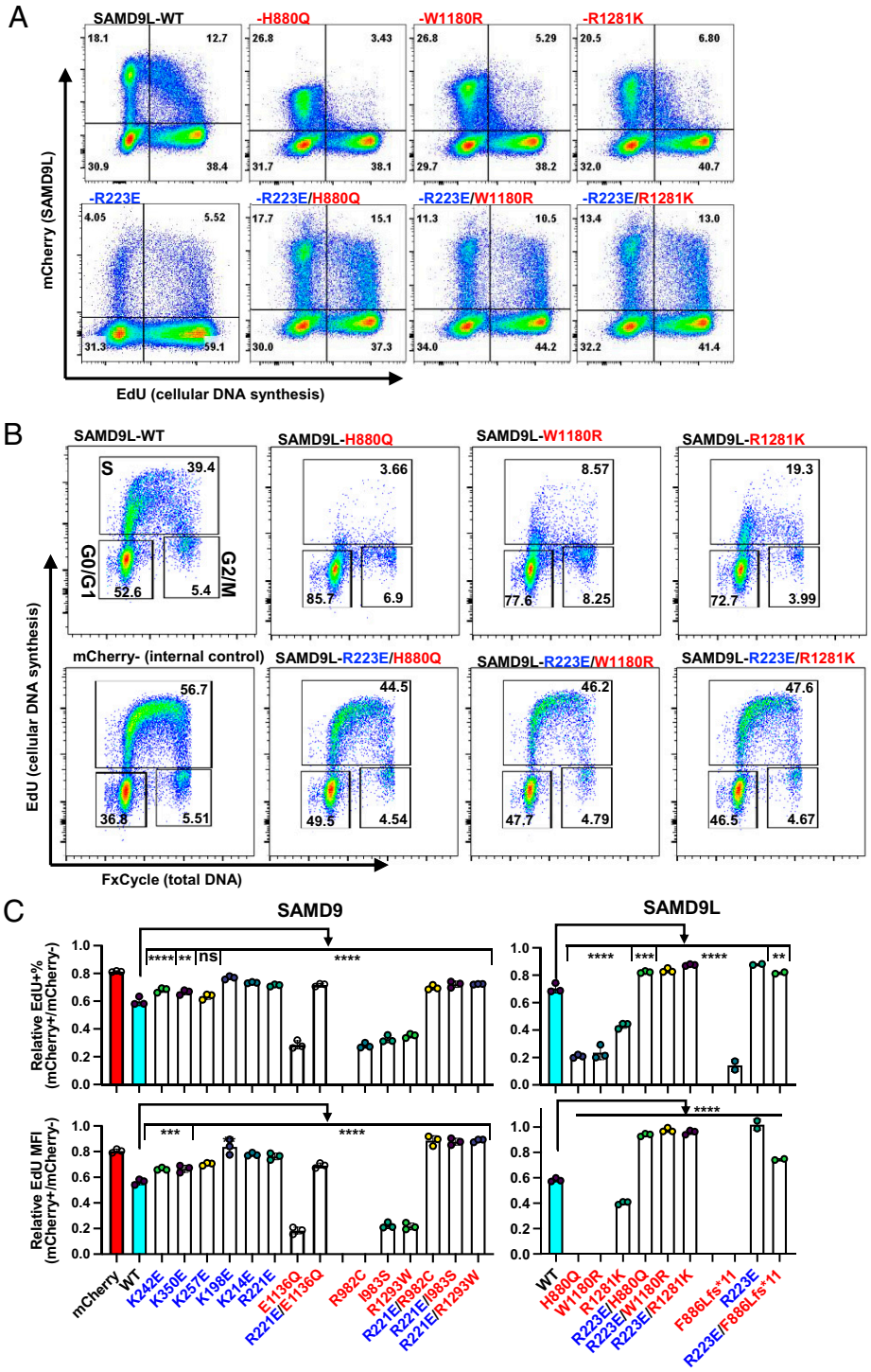

Fig. 3. dsNA binding by DBD is essential for antiproliferative activities of the WT and GoF SAMD9/9L variants. mCherry-SAMD9/9L mutants as illustrated in Fig. 2*A* were transfected into HEK 293T cells for 24 h, and the total and newly synthesized cellular DNA were labeled with FxCycle and EdU (for 2 h), respectively. Representative flow cytometry plots of cellular EdU and mCherry levels in the total cell population (*A*), or cellular EdU and FxCycle levels among mCherry-SAMD9L^{+} or mCherry^{-} population. (*B*) Relative S-phase (*C*, *Upper*) and DNA synthesis levels (*C*, *Lower*) between SAMD9-expressing and nontransfected cells from the same culture wells are derived from the flow cytometry data shown in Fig. 3 and *SI Appendix*, Fig. S6. Each biological replicate and SD are shown. Statistics: one-way ANOVA compared to the WT (ns, not significant; $^{**}P < 0.01$; $^{****}P < 0.0001$).

and F886Lfs*11 of SAMD9L demonstrating the strongest effect (Fig. 3*C*), nearly preventing cells from synthesis of DNA. The GoF variants reduced cellular DNA synthesis even at low expression levels, and the cell cycle stalled primarily at the G0/G1 phase (Fig. 3*B* and *SI Appendix*, Fig. S6).

Like their effects on antiviral activities, the DBD-defective K198E, K214E, and R221E mutations inactivated, while K242E, K257E, and K350E mutations reduced the antiproliferative activity of the WT SAMD9 (Fig. 3*C* and *SI Appendix*, Fig. S6*B*). A similar effect was observed when the DBD mutations were combined with SAMD9^{R982C}, except that the magnitude of change was even greater (*SI Appendix*, Fig. S6 *C–E*), as the GoF variant had a much stronger antiproliferative activity than the WT. For all the other GoF SAMD9/9L variants we have tested, including the frameshifted SAMD9L^{F886Lfs*11}, their antiproliferative activities were abolished by combining with the DBD-defective SAMD9^{R221E} or SAMD9L^{R223E} mutation (Fig. 3*C* and *SI Appendix*, Fig. S6).

GoF SAMD9/9L Variants Inhibit Global Protein Synthesis and Induce Proteotoxic Stress Response. A shut-off of cellular protein synthesis is associated with abortive viral replication caused by SAMD9 (19, 24), so we studied whether SAMD9/9L had a direct effect on cellular protein synthesis. Metabolic labeling with a methionine analog in SAMD9-transduced BT20 cells did not reveal any obvious effect of the WT SAMD9 on cellular protein synthesis. However, a GoF SAMD9 variant, R1293W, greatly reduced global protein synthesis after SAMD9 expression was specifically induced for more than 6 h (Fig. 4*A* and *SI Appendix*, Fig. S7*A*). Analysis of the total cellular RNA and the transcriptome showed that RNA integrity and transcription of vast majority of the cellular genes were not affected by the GoF variant (Fig. 4*B* and *SI Appendix*, Fig. S7*B* and Dataset S1). A total of 43 genes were significantly induced (Fig. 4*B* and *SI Appendix*, Fig. S7*C*), and gene ontology analysis indicated that they belong to the pathways of unfolded protein response or the responses to various eIF2-α kinases, indicating that the GoF variant caused a proteotoxic stress response.

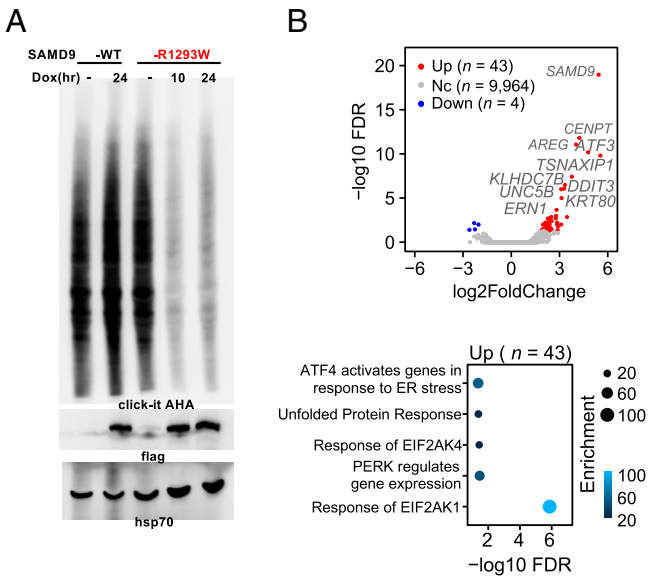

Fig. 4. GoF SAMD9 R1293W variant inhibits global protein synthesis and induces proteotoxic stress responses. BT20 cell lines that stably express either the WT or R1293W SAMD9 under the control of a doxycycline (Dox) inducible promoter were established. (*A*) After the cells were induced with Dox for the indicated hours, nascent cellular protein synthesis rate was measured by metabolic labeling with L-azidohomoalanine (AHA) for 2 h. SAMD9 expression is indicated by immunoblot against the Flag epitope tag, while similar loading levels are indicated by immunoblot against HSP70. (*B*) Transcriptome analysis of BT20 cells that were uninduced or induced to express SAMD9^{R1293W} for 24 h. *Upper*: a volcano plot showing genes with significantly up- (red) and down- (blue) regulated mRNA levels upon expression of SAMD9^{R1293W}. Genes with no significant change were shown as gray. *Lower*: a dot plot showing enriched pathways of significantly up-regulated genes. Enrichment of each pathway was coded by color and size of circles.

To quantify the effect of additional SAMD9/9L variants on global protein synthesis, we transiently transfected the variants into 293T cells and fluorescently labeled nascent cellular proteins with a puromycin analog. Flow cytometry analysis showed that the WT SAMD9/9L did not reduce cellular protein synthesis until their cellular expression reached a very high level (Fig. 5*A*, *Upper*). By contrast, the GoF SAMD9/9L mutants reduced protein synthesis in nearly all transfected cells, and the level of reduction correlated with SAMD9/9L expression level (Fig. 5*A* and *SI Appendix*, Fig. S8). Moreover, the effects of the GoF variants on protein synthesis correlate with the strength of their antiproliferative activities, with SAMD9^{R982C}, SAMD9L^{H880Q}, and SAMD9L^{F886Lfs*11} displaying the strongest effect (Fig. 5 and *SI Appendix*, Fig. S8). Overall, the quantitative flow cytometry analysis indicated that the GoF variants as well as a high cellular level of the WT SAMD9/9L had an inhibitory effect on cellular protein synthesis.

DBD dsNA Binding Activity Is Essential for SAMD9/9L to Inhibit Global Protein Synthesis and Reduce Translation Elongation. In contrast to the WT and GoF SAMD9/9L variants, the DBD-defective K198E, K214E, and R221E mutants as well as the K257E mutant had no inhibitory effect on cellular protein synthesis, while the DBD partially defective K242E and K350E mutants had a small inhibitory effect only when they were expressed at a very high level (Fig. 5*B* and *SI Appendix*, Fig. S8). More strikingly, the strong inhibitory effect of the GoF variants on cellular protein synthesis was abolished when they were combined with the DBD-defective SAMD9^{R221E} or SAMD9L^{R223E} mutation, resulting in similar levels of cellular protein synthesis in all cells regardless of the SAMD9/9L expression levels (Fig. 5 and *SI Appendix*, Fig. S8). Similar rescuing effects could even be detected from the total cell population by Western blot of puromycin-labeled proteins (*SI Appendix*, Fig. S9).

The effects of the SAMD9/9L mutants on cellular protein synthesis were also evident from quantitative analysis of SAMD9/9L protein levels in transfected cells. Mean fluorescence intensity (MFI) of various mCherry-SAMD9/9L GoF variants in transfected cells was significantly lower than that of the WT, which in turn was greatly reduced compared to that of the DBD mutants (*SI Appendix*, Fig. S10), despite only a few nucleotides difference between the constructs. The DBD-defective K198E, K214E, and R221E mutants had the highest MFI, while K350E, K242E, and K257E mutants had the intermediate MFI (*SI Appendix*, Fig. S10), correlating with the effects of the mutations on antiproliferative activities. Combining the DBD-defective SAMD9^{R221E} or SAMD9L^{R223E} mutation with the GoF variants greatly increased the protein level from that of the GoF variants (*SI Appendix*, Fig. S10*B*).

A recent study showed that some GoF SAMD9L variants inhibited translation elongation (6). To determine whether SAMD9 has a similar effect, we performed a modified "SunRiSE" assay that measures ribosome run-off with flow cytometry at single-cell resolution (25). Compared to nontransfected cells in the same culture well, cells expressing SAMD9 were slightly slower in ribosome run-off after new translation initiation was blocked with an inhibitor, resulting in a smaller reduction in active translation at 30 s post the initiation block (Fig. 5*C*). Ribosome run-off was slowed even further in cells expressing SAMD9^{R1293W}, while it was not affected by

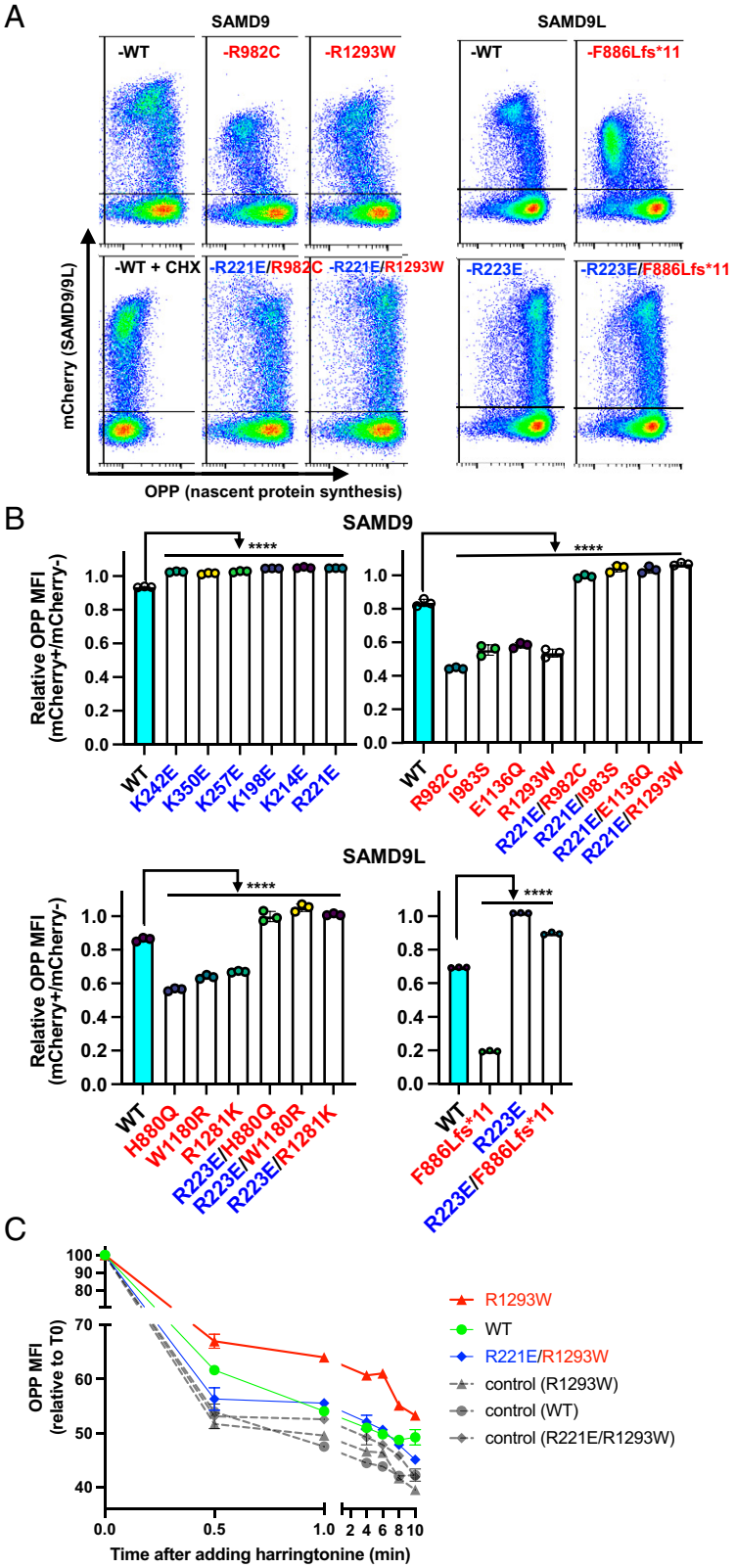

Fig. 5. dsNA binding by DBD is essential for SAMD9/9L to inhibit global protein synthesis and reduce translation elongation. (*A*) HEK 293T cells were transfected with mCherry-SAMD9/9L mutants as illustrated in Fig. 2*A* and labeled with OPP for 30 min. Representative flow cytometry plots of OPP level relative to cellular mCherry level are shown. Background level of OPP staining in cells that were treated with cycloheximide (CHX) is shown as a control. (*B*) Nascent protein synthesis levels in SAMD9/9L-expressing cells relative to nontransfected cells from the same culture wells are derived from the flow cytometry data shown in Fig. 5 and *SI Appendix*, Fig. S8. Each replicate and SD are shown. Statistics: one-way ANOVA compared to the WT (****$P < 0.0001$). (*C*) Identically transfected cells were treated with harringtonine to block new translation initiation. Active protein synthesis level at the indicated times after harringtonine treatment was assessed by measuring OPP level as described in (*A*) and normalized to the level at time 0 (T0). Each data point represents the average and SD of duplicate samples.

SAMD9$^{R221E/R1293W}$, indicating that the GoF SAMD9 variant inhibits translation elongation in a manner that also requires the DBD activity.

Discussion

In this study, we revealed the structure and function of a domain that is essential not only for the physiological functions of SAMD9/9L but also for the pathogenic effects exerted by the GoF variants identified in a myriad of human diseases. The GoF variants we have analyzed encompass all mutation types identified in human patients so far, including the frameshift and missense mutations in the putative NTPase domain and the rest of the C-terminal half. Amazingly, single substitution of a key basic residue in DBD completely abrogate the deleterious effects caused by every GoF variant tested, suggesting that modulating DBD activity could be a therapeutic strategy for various diseases caused by those variants.

The crystal structure of SAMD9-DBD:DNA complex revealed a compact domain that primarily engages the DNA backbone in a sequence-independent manner. Although an Alba domain was predicted for SAMD9, our study identified a domain that is more than 70 aa larger than the predicted Alba domain, with a more complex structure than the canonical β-α-β-α-β-β Alba fold (22). Furthermore, the DNA contact surface in the SAMD9-DBD:DNA structure is different from that of the existing Alba:DNA structures. In a structure of archaeal chromatin protein Alba2 domain (PDB code: 3U6Y) (26), the key DNA-contacting residues are predominantly located on the loops and the tip of helix α-2, with no involvement from α-1. By contrast, two of the three key contacting residues in SAMD9 (K214 and R221) are located on helix α-1, and α-2 is not involved.

Although the solved structure is of a complex with DNA, our EMSA data showed that the recombinant DBD can also bind dsRNA. The binding affinity of DBD with a model DNA substrate is relatively weak (K_D = 16 μM). Considering their cytoplasmic site of action and the recently reported interactions with ribosomal components (27), SAMD9/9L may bind to double-stranded regions of cytoplasmic RNA such as ribosomal RNA. Since the antiproliferative effect depends on the NA binding, DBD binding of NA in full-length SAMD9/9L is likely subject to tight regulation by other domains or cellular partners. Notably, SAMD9/9L also have a predicted protein deacetylase domain (SIR2) that may regulate NA binding by deacetylating lysine residues (21). What NA SAMD9/9L bind in cells and how the binding is regulated remain to be determined.

Guided by the complex structure, we were able to precisely perturb the dsNA binding activity without affecting the overall structure, which allowed us to demonstrate that the dsNA binding activity is essential for the known functions of SAMD9/9L. Significantly, the different effects the mutations have on SAMD9/9L functions largely correlate with their effects on DNA binding, indicating that the effector functions are closely linked to the dsNA binding activity. SAMD9/9L are large, multidomain proteins, so it would not be surprising if they had separate effector domains for their diverse functions in antiviral defense and tumor suppression. However, we showed that the same NA binding residues are essential for both the antiviral and antiproliferative functions, suggesting that the two functions share at least one common molecular mechanism that requires dsNA binding by DBD. As one mutation (K257E) in DBD was found to disrupt SAMD9 functions without affecting NA binding, dsNA binding by DBD is necessary but not sufficient for the SAMD9/9L functions.

What might be the common molecular process underlying the antiviral and antiproliferative functions of SAMD9/9L? While dysregulation of endocytosis has been the main mechanism proposed for the antiproliferative function (1, 11), protein synthesis shutoff was recognized as the hallmark for host restriction of vK1$^-$C7$^-$ (19), long before SAMD9/9L were discovered to be the culprits. We thus have focused on translational control as the potential underlying mechanism and found that GoF SAMD9/9L variants profoundly inhibit global protein synthesis. Several papers recently reported a similar inhibitory effect of the GoF variants on cellular protein synthesis while our manuscript was being prepared (6, 7, 27). We showed further that the same DBD residues that are essential for the antiviral and antiproliferative activities are also critical for SAMD9/9L to inhibit protein synthesis, suggesting that translational control is an important underlying mechanism for SAMD9/9L functions. How SAMD9/9L inhibit protein synthesis is unclear, but we found that a GoF SAMD9 variant induces a proteotoxic stress response that resembles the closest with the response of EIF2AK1. While PKR (EIF2AK2) was previously shown to be dispensable for SAMD9 antiviral activities (24, 28), whether other eIF2-α kinases are involved in SAMD9/9L functions is yet to be determined. Beyond a potential effect on translation initiation possibly through modulating eIF2-α, SAMD9L was shown recently (6), and SAMD9 was shown here, to reduce translation elongation. The DBD activity is also required for this process, but the mechanism is unknown.

There is one notable difference in SAMD9/9L activities under noninfectious and infectious conditions. Under noninfectious condition, GoF variants are much more potent than the WT at inhibiting cell growth and cellular protein synthesis. By contrast, the WT and GoF variants are equally effective at inhibiting vaccinia virus replication. Since the GoF variants inhibit cellular protein synthesis in uninfected cells, their antiviral effects could simply reflect a preexisting block in translation when the infection occurs. The WT on the other hand has a minor effect on cellular protein synthesis in uninfected cells, but it achieves a similar level of viral inhibition as the GoF variants, suggesting that the WT is not intrinsically less active than the GoF variants. Rather, the relative minor effect of the WT under noninfectious conditions is probably due to an autoinhibitory effect, which is relieved by viral infection. GoF mutations probably disrupt the autoinhibitory mechanism. Specifically, the C-terminal half that is truncated by the frameshift GoF SAMD9L variant is likely involved in the autoinhibition. Our findings that the dsNA binding residues are required even for the activities of the frameshift variant again illustrate that DBD is a key effector domain and its dsNA binding activity is an essential effector function.

Materials and Methods

Recombinant SAMD9$^{134-385}$ or SAMD9$^{156-385}$ protein was expressed in *Escherichia coli* as a SUMO fusion with a 6xHis-tag and purified by nickel nitrilotriacetic acid (Ni-NTA) as previously described (29). The complex of SAMD9$^{156-385}$ and a 22-nt dsDNA was crystalized in a solution containing 0.1 M Hepes, pH 7.5, 0.2 M ammonium acetate (NH_4AC), 20 mM $MgCl_2$, and 20% PEG3350. Diffraction data from a selenomethionine-substituted protein crystal were used to obtain an initial structure by the single-wavelength-anomalous-dispersion method, while data from a native protein crystal were used to obtain a higher-resolution structure by the molecular replacement method. The binding of the purified SAMD9 proteins with a 5′ 6-FAM–labeled 22-nt dsDNA was studied by EMSA on a 0.8% native agarose gel. Affinities were obtained by nonlinear regression curve fitting of the fluorescence polarization data. Plasmids for transient expression of mCherry and SAMD9/9L fusions, pcDNA6.2/mCherry-SAMD9/9L, were a generous gift of Jeffery M. Klco, St. Jude Research Hospital, Memphis, TN (27). Specific mutations of SAMD9/9L were introduced into the plasmids through recombinant PCR-based site-directed mutagenesis as described previously (30). The plasmids were transfected into HEK 293T cells for 24 to 36 h. For assessing antiviral activities, the transfected cells were infected with vK1$^-$C7$^-$/GFP$^+$ (20, 28, 30) for 15 h. For assessing antiproliferative activities, the transfected cells were treated with 5-ethynyl-2′-deoxyuridine (EdU) for 2 h before they were processed with Click-iT Plus EdU Alexa Fluor 488 Flow Cytometry Assay Kit (Thermo Fisher Scientific). For assessing protein synthesis level, transfected cells were treated with O-propargyl-puromycin (OPP) for 30 min before they were processed with Click-iT Plus OPP Alexa Fluor 488 Protein

Synthesis Assay Kit (Thermo Fisher Scientific). For assessing protein elongation rate, identically transfected cells were treated with 2 μg/mL Harringtonine (LKT Laboratories, Inc.) for various times before the cellular protein synthesis level was assessed with Click-iT Plus OPP kit. Flow cytometry analysis was performed with an LSR-II cell analyzer (BD Biosciences). For RNA-seqencing (RNA-seq) analysis, BT20 cells transduced with SAMD9-R1293W were uninduced or induced with 2 μg/mL doxycycline for 24 h. Messenger RNA (mRNA) was isolated from the cells and processed for DNA library construction with NEBNext Ultra RNA Library Prep Kit for Illumina (NEB). RNA-seq reads were mapped to the human transcriptome and counted for each transcript. The count table was analyzed by DESeq2 (31), and the significantly changed mRNAs were analyzed by PANTHER (32) to search enriched pathways. The more detailed materials and methods can be found in *SI Appendix, Materials and Methods*.

Data Availability. Crystal structure data have been deposited in Protein Data Bank (Accession No. 7ksp). RNA-seq data have been deposited in Gene Expression Omnibus (GSE186456). All other study data are included in the article and/or supporting information.

ACKNOWLEDGMENTS. We thank the staff of beam-line 19ID at the Advanced Photon Source for their support and Dr. Jeffery M. Klco for providing plasmids. This work was supported by NIH Grant No. AI151638 (Y.X.). J.D. is also supported by the Oklahoma Agricultural Experiment Station at Oklahoma State University under Project No. OKL03060. Flow cytometry data were generated in the University of Texas (UT) Health San Antonio Flow Cytometry Shared Resource Facility (supported by Grant Nos. NIH P30 CA054174 and UL1 TR002645) with the help from Sebastian Montagnino. Sequencing data were generated in the UT Health San Antonio Genome Sequencing Facility (supported by Grant Nos. NIH P30 CA054174 and 1S10OD021805-01).

1. S. Narumi *et al.*, SAMD9 mutations cause a novel multisystem disorder, MIRAGE syndrome, and are associated with loss of chromosome 7. *Nat. Genet.* **48**, 792–797 (2016).
2. D. H. Chen *et al.*, Ataxia-pancytopenia syndrome is caused by missense mutations in SAMD9L. *Am. J. Hum. Genet.* **98**, 1146–1158 (2016).
3. B. Tesi *et al.*, Gain-of-function *SAMD9L* mutations cause a syndrome of cytopenia, immunodeficiency, MDS, and neurological symptoms. *Blood* **129**, 2266–2279 (2017).
4. J. R. Schwartz *et al.*, The genomic landscape of pediatric myelodysplastic syndromes. *Nat. Commun.* **8**, 1557 (2017).
5. A. A. de Jesus *et al.*, Distinct interferon signatures and cytokine patterns define additional systemic autoinflammatory diseases. *J. Clin. Invest.* **130**, 1669–1682 (2020).
6. E. J. Allenspach *et al.*, Germline SAMD9L truncation variants trigger global translational repression. *J. Exp. Med.* **218**, e20201195 (2021).
7. A. J. Russell *et al.*, SAMD9L autoinflammatory or ataxia pancytopenia disease mutations activate cell-autonomous translational repression. *Proc. Natl. Acad. Sci. U.S.A.* **118**, e2110190118 (2021).
8. F. Buonocore *et al.*, Somatic mutations and progressive monosomy modify SAMD9-related phenotypes in humans. *J. Clin. Invest.* **127**, 1700–1713 (2017).
9. T. Inaba, H. Honda, H. Matsui, The enigma of monosomy 7. *Blood* **131**, 2891–2898 (2018).
10. J. Davidsson *et al.*, SAMD9 and SAMD9L in inherited predisposition to ataxia, pancytopenia, and myeloid malignancies. *Leukemia* **32**, 1106–1115 (2018).
11. A. Nagamachi *et al.*, Haploinsufficiency of SAMD9L, an endosome fusion facilitator, causes myeloid malignancies in mice mimicking human diseases with monosomy 7. *Cancer Cell* **24**, 305–317 (2013).
12. X. Meng *et al.*, A paralogous pair of mammalian host restriction factors form a critical host barrier against poxvirus infection. *PLoS Pathog.* **14**, e1006884 (2018).
13. G. Sivan, P. Ormanoglu, E. C. Buehler, S. E. Martin, B. Moss, Identification of restriction factors by human genome-wide RNA interference screening of viral host range mutants exemplified by discovery of SAMD9 and WDR6 as inhibitors of the vaccinia virus K1L-C7L-mutant. *MBio* **6**, e01122 (2015).
14. J. Liu, S. Wennier, L. Zhang, G. McFadden, M062 is a host range factor essential for myxoma virus pathogenesis and functions as an antagonist of host SAMD9 in human cells. *J. Virol.* **85**, 3270–3282 (2011).
15. C. F. Li *et al.*, Human sterile alpha motif domain 9, a novel gene identified as down-regulated in aggressive fibromatosis, is absent in the mouse. *BMC Genomics* **8**, 92 (2007).
16. B. Nounamo *et al.*, An interaction domain in human SAMD9 is essential for myxoma virus host-range determinant M062 antagonism of host anti-viral function. *Virology* **503**, 94–102 (2017).
17. F. Zhang, X. Meng, M. B. Townsend, P. S. Satheshkumar, Y. Xiang, Identification of CP77 as the third orthopoxvirus SAMD9 and SAMD9L inhibitor with unique specificity for a rodent SAMD9L. *J. Virol.* **93**, e00225-19 (2019).
18. J. C. Hsiao, C. S. Chung, R. Drillien, W. Chang, The cowpox virus host range gene, CP77, affects phosphorylation of eIF2 alpha and vaccinia viral translation in apoptotic HeLa cells. *Virology* **329**, 199–212 (2004).
19. R. Drillien, F. Koehren, A. Kirn, Host range deletion mutant of vaccinia virus defective in human cells. *Virology* **111**, 488–499 (1981).
20. X. Meng, J. Chao, Y. Xiang, Identification from diverse mammalian poxviruses of host-range regulatory genes functioning equivalently to vaccinia virus C7L. *Virology* **372**, 372–383 (2008).
21. S. L. Mekhedov, K. S. Makarova, E. V. Koonin, The complex domain architecture of SAMD9 family proteins, predicted STAND-like NTPases, suggests new links to inflammation and apoptosis. *Biol. Direct* **12**, 13 (2017).
22. M. Goyal, C. Banerjee, S. Nag, U. Bandyopadhyay, The Alba protein family: Structure and function. *Biochim. Biophys. Acta* **1864**, 570–583 (2016).
23. E. Krissinel, K. Henrick, Secondary-structure matching (SSM), a new tool for fast protein structure alignment in three dimensions. *Acta Crystallogr. D Biol. Crystallogr.* **60**, 2256–2268 (2004).
24. G. Sivan, S. G. Glushakow-Smith, G. C. Katsafanas, J. L. Americo, B. Moss, Human host range restriction of the vaccinia virus C7/K1 double deletion mutant is mediated by an atypical mode of translation inhibition. *J. Virol.* **92**, e01329-18 (2018).
25. R. J. Argüello *et al.*, SunRiSE—Measuring translation elongation at single-cell resolution by means of flow cytometry. *J. Cell Sci.* **131**, jcs214346 (2018).
26. T. Tanaka, S. Padavattan, T. Kumarevel, Crystal structure of archaeal chromatin protein Alba2-double-stranded DNA complex from *Aeropyrum pernix* K1. *J. Biol. Chem.* **287**, 10394–10402 (2012).
27. M. E. Thomas, 3rd *et al.*, Pediatric MDS and bone marrow failure-associated germline mutations in SAMD9 and SAMD9L impair multiple pathways in primary hematopoietic cells. *Leukemia* **35**, 3232–3244 (2021).
28. X. Meng *et al.*, Vaccinia virus K1L and C7L inhibit antiviral activities induced by type I interferons. *J. Virol.* **83**, 10627–10636 (2009).
29. B. Krumm, X. Meng, Y. Li, Y. Xiang, J. Deng, Structural basis for antagonism of human interleukin 18 by poxvirus interleukin 18-binding protein. *Proc. Natl. Acad. Sci. U.S.A.* **105**, 20711–20715 (2008).
30. X. Meng, Y. Xiang, Vaccinia virus K1L protein supports viral replication in human and rabbit cells through a cell-type-specific set of its ankyrin repeat residues that are distinct from its binding site for ACAP2. *Virology* **353**, 220–233 (2006).
31. M. I. Love, W. Huber, S. Anders, Moderated estimation of fold change and dispersion for RNA-seq data with DESeq2. *Genome Biol.* **15**, 550 (2014).
32. H. Mi, A. Muruganujan, D. Ebert, X. Huang, P. D. Thomas, PANTHER version 14: More genomes, a new PANTHER GO-slim and improvements in enrichment analysis tools. *Nucleic Acids Res.* **47** (D1), D419–D426 (2019).